GSA DATA REPOSITORY 2017157

Synconvergent exhumation of metamorphic core complexes in the northern North American Cordillera

Liane M. Stevens*, Rebecca Bendick, and Julia A. Baldwin

APPENDIX DR1. EXTENDED DESCRIPTION OF NUMERICAL SIMULATIONS

The numerical simulations used in this study are built with the COMSOL multiphysics finite element solver including the arbitrary Lagrangian-Eulerian (ALE) formulation (Fullsack, 1995) to accommodate large deformation and erosion on the upper boundary of the model domain. The specifics of the model setup are described below.

ALE

All of the model domain boundaries are fixed in space. Mass may be advected through the top boundary only; once mass passes through the $z = z_{max}$ surface (the Earth's surface), it disappears from the computation. Therefore, the top temperature and velocity boundary conditions are always applied on $z = z_{max}$ (100 km). Total mass is conserved such that the sum of the flux out of the upper surface and the outflow over the craton margin equals the inflow at x = 0 (Fig. DR1).

Fluid mechanics

The velocity field is calculated for a viscous fluid on the model domain using the Navier-Stokes equation where the inertial terms are assumed to equal zero (laminar flow), $\rho\frac{\partial \boldsymbol{u}}{\partial t} = \nabla \cdot [-\rho + \mu(\nabla \boldsymbol{u} + (\nabla \boldsymbol{u})^{\boldsymbol{T}})] + \boldsymbol{F}$ with $\rho\nabla \cdot \boldsymbol{u} = 0$. In this expression, ρ is the fluid density, $\boldsymbol{u}$ is the velocity vector, μ is the viscosity, and **F** is the body force tensor.

The upper boundary at $z = z_{max}$ is free, so that fluid can move through $z = z_{max}$ (45 km) to form topography (or be "eroded" using the ALE formulation). The outflow condition is a free boundary, where fluid can move out of the model domain. The y = 0 and $y = y_{max}$ (800 km) boundaries have free boundary-parallel slip, and the basal boundary, including the top surface of the craton margin, has a fixed velocity boundary condition set at the inflow velocity to approximate net convergence between the craton and the overriding accreted crust (Fig. DR1). The viscosity of the fluid (Fig. DR5) in the model domain is either constant (in the constant viscosity simulations, Table DR2), or determined by the temperature solution for the domain, through $\eta = \frac{1}{2}A^{-1/n}\dot{\varepsilon}^{1-n/n}exp\left(\frac{Q}{nRT}\right)$, with varying values for n used in the sensitivity testing (Table DR2). In this expression, η is the viscosity, A is a conditioning coefficient, n is a viscosity exponent, $\dot{\varepsilon}$ is the strain rate, Q is the activation energy, R is the ideal gas constant, and T is the temperature.

Temperature

The temperature field is calculated for a viscous fluid including both advection and diffusion with the advection-diffusion equation, $\rho C_p \frac{\partial T}{\partial t} + \rho C_p \boldsymbol{u} \cdot \nabla T = \nabla \cdot (k \nabla T) + Q$. In this expression, ρ is the fluid density, C_p is the heat capacity, T is the temperature, t is time, $\boldsymbol{u}$ is the velocity vector, k is the thermal diffusivity, and Q is internal heat production. The initial temperature condition on the model domain is a 1D steady state continental geotherm for the boundary conditions specified below, no heat advection, and with internal heat production given by $Q = S_0 exp\left(\frac{-z}{h_r}\right)$. This temperature relation is also imposed on the inflow boundary (x = 0) for the duration of the model run. The outflow condition is free in the temperature problem. The y = 0 and $y = y_{max}$ boundaries are

insulated, so the net lateral heat flux equals zero. The geotherm between the uppermost and bottom boundaries is static, but we test a range of upper and lower boundary absolute temperature conditions from 30ºC on the top and 550ºC at the base (no uppermost crustal lid) to 230ºC on the top and 750ºC at the base (~8 km of overlying elastic crust). We adjust the basal and surface pressure condition accordingly in the cases with a lid.

The temperature on the top of the craton (Fig. DR1) at different depths is given by the solution (Molnar and England, 1990) for the steady state limit on a slipping discontinuity, $T' = \frac{T}{1+b\sqrt{(z_f V sin\delta)/\kappa}}$. In this expression, T' is the steady state temperature on the "fault", when T is the standard geothermal temperature for the given depth, b is a dimensionless correction factor, z_f is the depth to the discontinuity, V is the slip rate, δ is the component of the dip of the fault in the thrust direction, and κ is the thermal diffusivity.

The initial mesh and the model conditions are also summarized in Figure DR1. The range of parameter values used in the sensitivity testing are given in Table DR2.

Geometry

We calculate the time dependent pressure, temperature, and velocity fields for the model domain for a range of craton geometries (Table DR2). The craton is always a segment of an ellipsoid, to avoid solution singularities at indenter corners.

***P-T-t* Paths**

We calculate depth-temperature-time for a set of particles moving though the model domain in a particular solution; these are assumed to represent the observed rock *P-T-t* results from geothermobarometry, geochronology, and thermochronometry. Particles are "released" at the inflow boundary and move through the model domain

according to the calculated velocity field at each time step. At each time step, their position in space and temperature are calculated, the former according to the velocity at the previous time step and the latter according to the temperature at the new particle position. This method assumes that there is no difference between the temperature of a virtual particle at some time step and its calculated thermal cooling age due to the thermodynamics of the mineral closure.

REFERENCES CITED

Fullsack, P., 1995, An arbitrary Lagrangian-Eulerian formulation for creeping flows and its application in tectonic models: Geophysical Journal International, v. 120, p. 1-23.

Molnar, P., and England, P., 1990, Temperatures, heat flux, and frictional stress near major thrust faults: Journal of Geophysical Research, v. 95, p. 4833-4856.

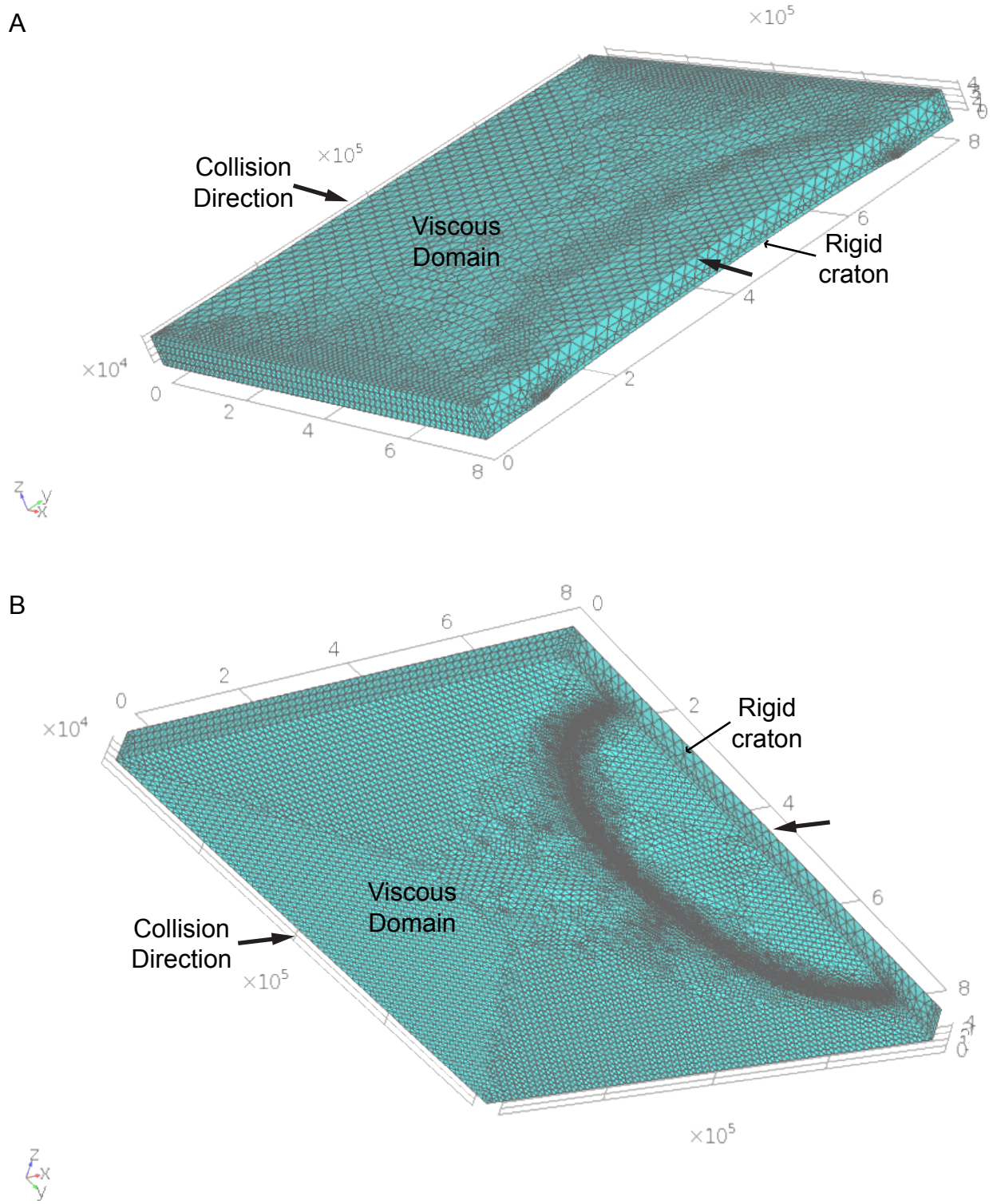

Figure DR1. Numerica model setup, including mesh geometry for the baseline model. A: Top view. B: Bottom view. See Figure 2 for additional boundary conditions.

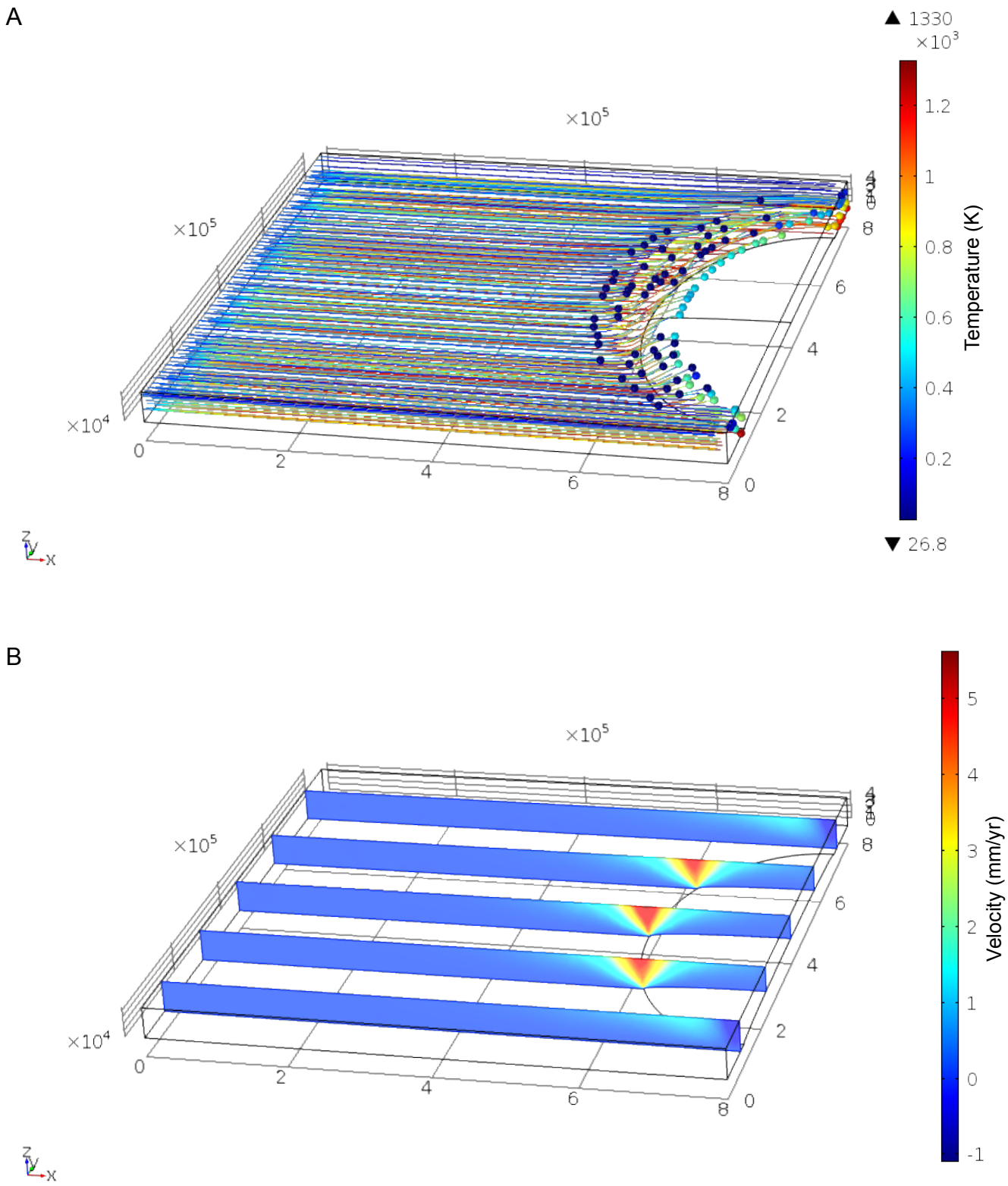

Figure DR2. Numerical model results. A: Particle paths converging with and exhumed at the front of a cratonic indenter. B: Vertical velocity slices through the model space.

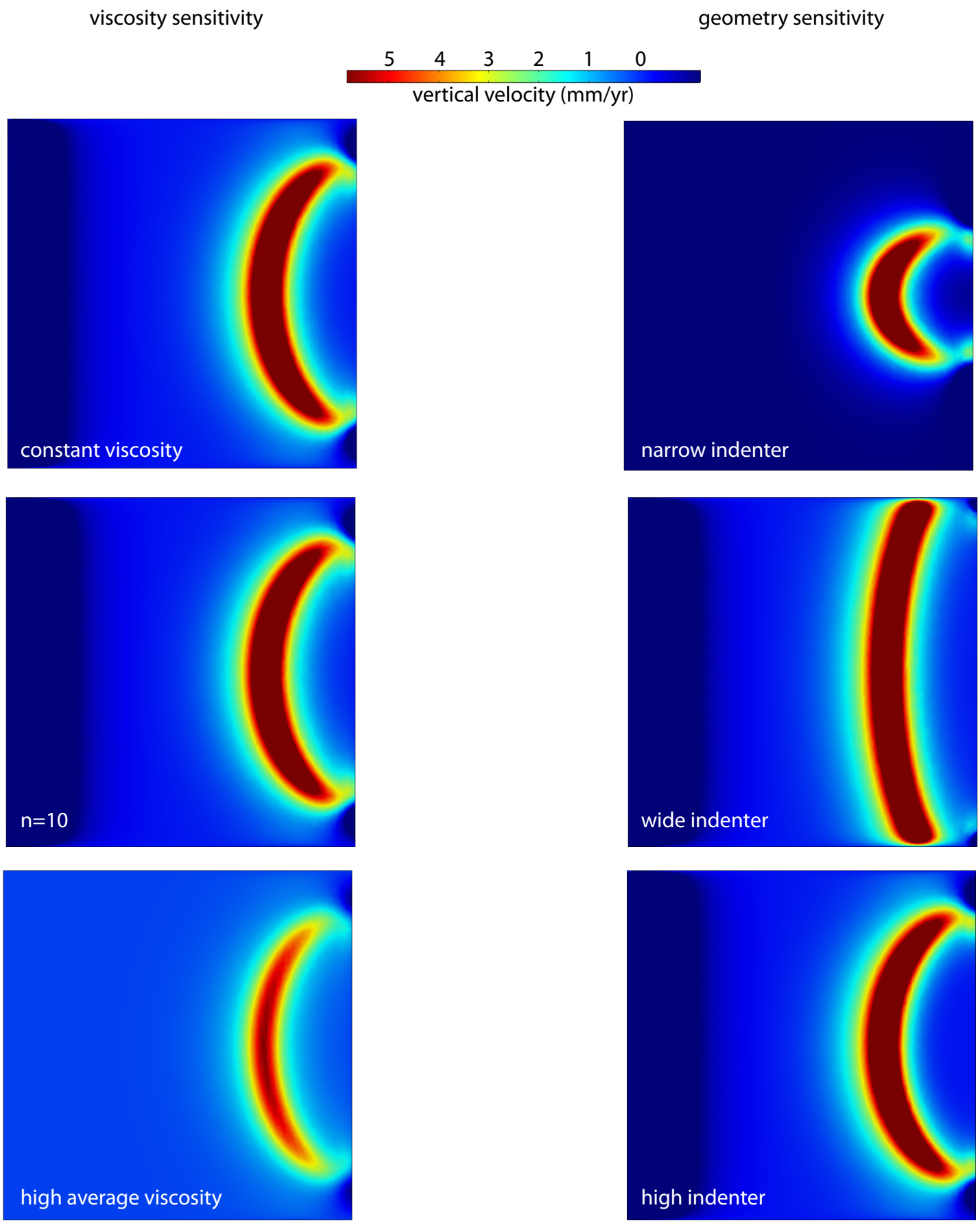

Figure DR3. Map view of vertical velocity at the surface of the model for non-preferred solutions. These illustrate the sensitivity of the model to variations in effective viscosity (left) and geometry (right).

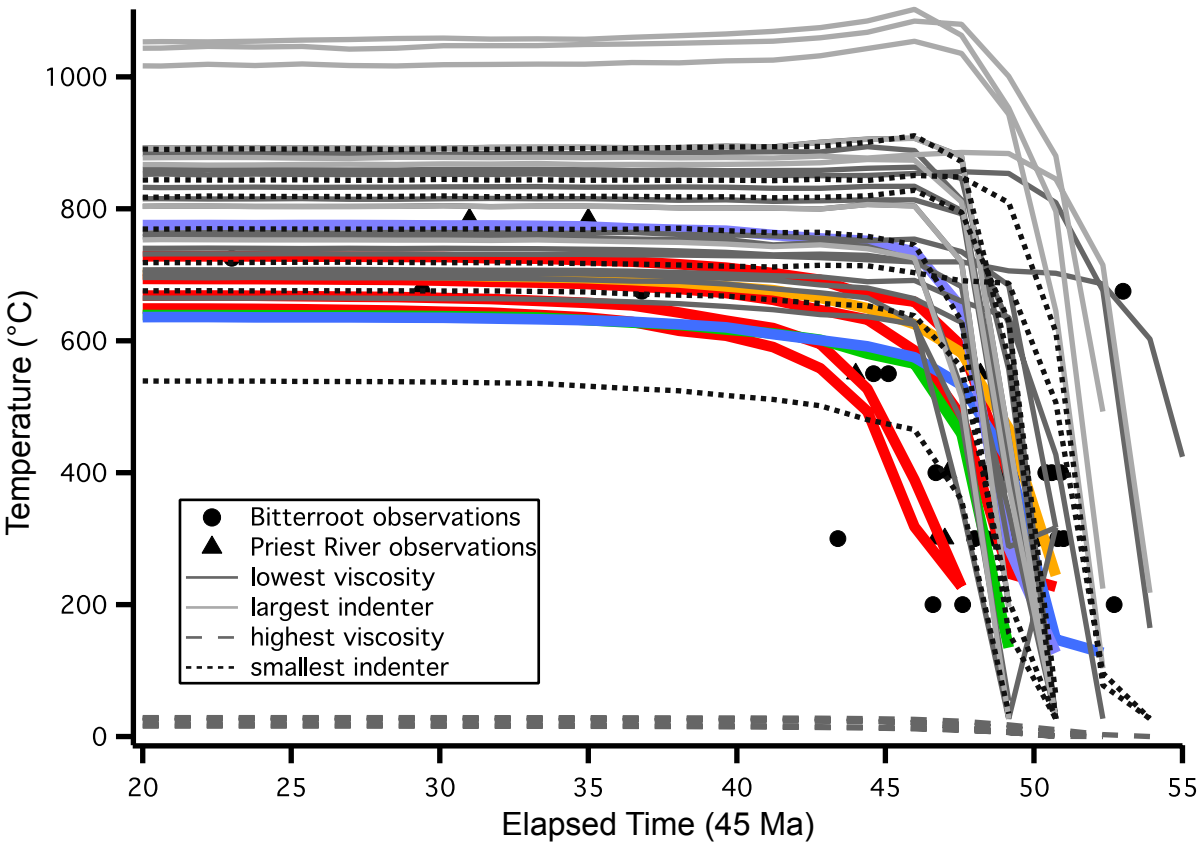

Figure DR4. Particle *T-t* paths for non-preferred solutions. A range of particle *T-t* paths from non-preferred, end member simulations (grays) are shown with particle *T-t* paths for preferred model solutions (colors) that are presented in the main text (Fig. 3B).

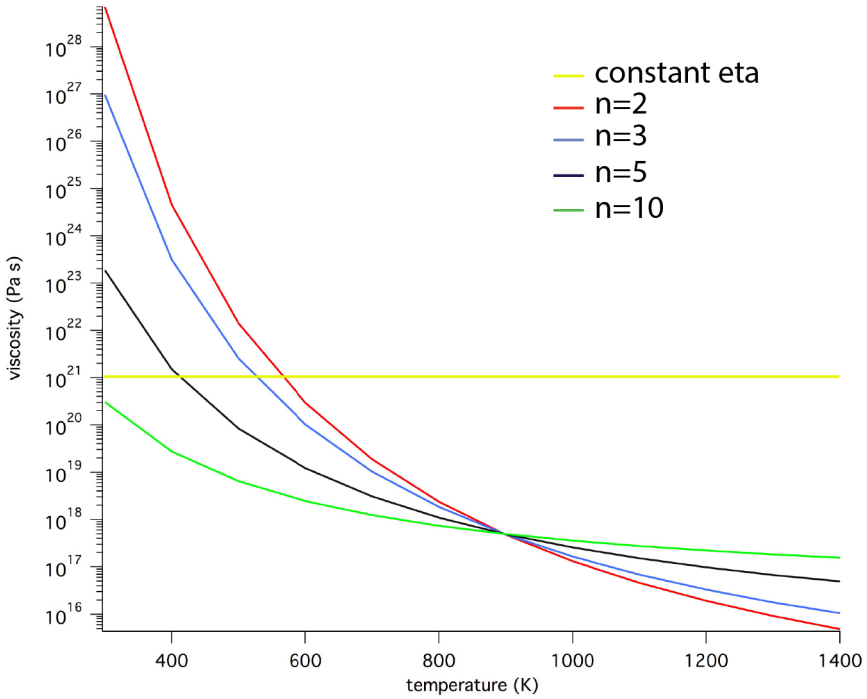

Figure DR5. Temperature-dependent viscosity laws. All of the viscosity relations except the constant viscosity case have the Arrhenius form; only the viscosity exponent varies. Larger values of n approach constant viscosity. In all cases, the average effective viscosity, given by the integral of the viscosity curve, is 10^{21} Pa.

Table DR1. Tectonic settings of metamorphic core complexes

Tectonic Setting	Complex	Location
Convergence:		
North American Cordillera		
	Shuswap	British Columbia
	Priest River	Idaho
	Clearwater	Idaho
	Bitterroot	Idaho, Montana
	Anaconda	Montana
	Pioneer	Idaho
	Albion-Grouse Creek-Raft River	Utah
	Ruby-Humboldt	Nevada
	Snake Range	Nevada
	Chemehuevi	California
	Whipple Mountains	California
	Buckskin-Rawhide	Arizona
	Harcuvar	Arizona
	Harquahala Mountains	Arizona
	South Mountains	Arizona
	Picacho	Arizona
	Catalina	Arizona
	Rincon	Arizona
	Sierra Mazatán	Sonora, Mexico
Alpine-Himalaya system		
	Lora del Río	Spain
	Sierra de las Estancias	Spain
	Tormes gneiss dome	Spain
	Massif Central	France
	Alpi Apuane	Italy
	Argentario Promontory	Italy
	Elba	Italy
	Giglio	Italy
	Monti Pisani	Italy
	Osogovo-Liset	Bulgaria
	Menderes	Turkey
	Niğde	Turkey
	Chapedony	Iran

	Delbar	Iran
	Kongur Shan	Pamirs
	Gurla Mandhata	Pamirs
	Ama Drime	Nepal
East and southeast Asia		
	Hohhot	China
	Hongzhen	China
	Liaonan	China
	Yagan-Onch Hayrhan	China
	Ziaoqinling	China
	Doi Inthanon	Thailand
	Malino	Indonesia
Extension:		
Backarc basin		
	Rhodope	Aegean, Greece
	Thasos	Aegean, Greece
	Tinos	Aegean, Greece
	Mykonos-Delos-Rhenia	Aegean, Greece
	Naxos	Aegean, Greece
	Ios	Aegean, Greece
	Kazdağ	Aegean, Turkey
Continental extension/Rifting		
	Paparoa	New Zealand
	Edough	Algero-Provencal basin, Algeria
Mid-ocean ridge/Spreading center		
	Atlantis Massif	Mid-Atlantic ridge
	Kane	Mid-Atlantic ridge
	Arctic	Mid-Atlantic ridge
	Mid-Cayman spreading center	Carribbean
	Godzilla	Parece Vela rift, western Pacific Ocean
	Atlantis Bank	Indian ridge
	D'Entrecasteaux Islands	Woodlark basin, Papua New Guinea
	Dayman Dome	Woodlark basin, Papua New Guinea
	Normanby Island	Woodlark basin, Papua New Guinea

Table DR2: Simulations, including best fitting (preferred) simulations, run during sensitivity testing.

Simulation Name	Collision velocity	Viscosity Exponent (n)	Indenter Width	Maximum indenter height from base of lithosphere
Variable Viscosity Simulations:				
Baseline	20 mm/yr	2	300 km	20 km
Constant Viscosity	20 mm/yr	no eta(T)	300 km	20 km
n3	20 mm/yr	3	300 km	20 km
n5	20 mm/yr	5	300 km	20 km
n10	20 mm/yr	10	300 km	20 km
high average eta	20 mm/yr	2, and A=10A	300 km	20 km
Variable Indenter Geometry Simulations:				
Wide Craton	20 mm/yr	2	500 km	20 km
Narrow Craton	20 mm/yr	2	150 km	20 km
High Craton	20 mm/yr	2	300 km	35 km
Low Craton	20 mm/yr	2	300 km	15 km
Very Low Craton	20 mm/yr	2	300 km	5 km
Variable Inflow Simulations:				
dU 2	20 mm/yr to 10 mm/yr	2	300 km	20 km
DU 10	20 mm/yr to 2 mm/yr	2	300 km	20 km
Best Fitting Simulations:				
Baseline + 8 km lid	20 mm/yr to 10 mm/yr	2	300 km	20 km
Low Craton + 4 km lid	20 mm/yr to 10 mm/yr	2	300 km	5 km
Hgh Eta + Low Craton + 4 km lid	20 mm/yr to 10 mm/yr	2, and A=10A	300 km	5 km

Table DR3. Preferred values for model parameters.

Parameter	Description	Preferred Value	Range Tested
u	collision rate	25 mm/yr	2.5-25 mm/yr
ρ	lithosphere density	2800 kg/m3	
Cp	heat capacity	800 J/kg K	
A	viscosity coefficient	1.00E-04	1e-4 to 1e-3
n	viscosity exponent	2	2-10
$\dot{e}$	strain rate	1.00E-18	
Q	activation energy	2.40E-05	
R	ideal gas constant	8.3	
S_0	volumetric heat production	5e-7 W/m3	
hr	skin depth	15 km	
Q_{moho}	Moho heat flux	0.032 W/m2	
Q_{surf}	surface heat flux	0.056 W/m2	
κ	thermal diffusivity	2 W/m K	
T_{base}	surface temperature	30°C	30°C - 230°C
T_{top}	basal temperature	650°C	550 °C - 750°C

Table DR4. Published temperature-time (*T-t*) data used to constrain *T-t* paths for deeply exhumed metamorphic core complexes in the northern North American Cordillera.

Summary	Complex	Temperature (°C)	Error	Date (Ma)	Error	Mineral	Fraction	Type	Method	Unit	Notes	Interpretation	Reference
Metamorphism	Bitterroot	700		64								peak metamorphism - M2 (high P)	House et al., 1997
Metamorphism	Bitterroot	700		64								peak metamorphism - M2 (low P)	House et al., 1997
Main Phase	Bitterroot	540		62.7	2.4	hornblende		40Ar/39Ar		Amphibolite, concordant, Spruce Creek mylonite zone (EM6)			House et al., 2002
Main Phase	Bitterroot	540		55.6	2.1	hornblende		40Ar/39Ar		Quartz diorite gneiss, Spruce Creek mylonite zone (EM3d)	isochron age		House et al., 2002
Main Phase	Bitterroot	300		54.2	0.6	biotite		40Ar/39Ar		Amphibolite, concordant, Spruce Creek mylonite zone (EM6)			House et al., 2002
Main Phase	Bitterroot	300		53.8	2	biotite		40Ar/39Ar		Quartz diorite gneiss, Spruce Creek mylonite zone (EM3d)			House et al., 2002
Main Phase	Bitterroot	200		53.3	1	k-feldspar		40Ar/39Ar		Granite pegmatite, cross cuts Spruce Creek mylonite zone (EM3b)			House et al., 2002
Extension/Challis	Bitterroot	200		52.4	2	k-feldspar		40Ar/39Ar		Skookum Butte biotite granite (NB12-11)			House et al., 2002
Extension/Challis	Bitterroot	300		50.2	1	biotite		40Ar/39Ar		Skookum Butte biotite granite (NB12-11)			House et al., 2002
Extension/Challis	Bitterroot	300		49.6	0.2	biotite		40Ar/39Ar		Lolo Hot Springs batholith; epizonal pluton	Plateau age		Foster et al., 2001
Extension/Challis	Bitterroot	300		49.3	1	biotite		40Ar/39Ar		Granite, concordant, Spruce Creek mylonite zone (EM3c)			House et al., 2002
Extension/Challis	Bitterroot	300		48.8	0.3	biotite		40Ar/39Ar		Skookum Butte pluton	Total fusion age		Foster et al., 2001
Extension/Challis	Bitterroot	400		48.7	0.5	muscovite		40Ar/39Ar		Granite pegmatite, cross cuts Spruce Creek mylonite zone (EM3b)	intercept age		House et al., 2002
Extension/Challis	Bitterroot	300		48.6	0.8	biotite		40Ar/39Ar		Whistling Pig pluton (B85)	intercept age	Rapid cooling after crystallization	House et al., 2002
Extension/Challis	Bitterroot	540		48.4	0.9	hornblende		40Ar/39Ar		amhibolite pod (NB5-1); concordant but not mylonitic	isochron age	Age of mylonitization	House & Hodges, 1994
Extension/Challis	Bitterroot	540		47.9	0.9	hornblende		40Ar/39Ar		amhibolite pod (NB17-1); concordant but not mylonitic	isochron age	Age of mylonitization	House & Hodges, 1994
Extension/Challis	Bitterroot	200		47.8	0.6	k-feldspar		40Ar/39Ar		Whistling Pig pluton (B85)	intercept age	Rapid cooling after crystallization	House et al., 2002
Extension/Challis	Bitterroot	200		47.5	0.3	k-feldspar		40Ar/39Ar		granodiorite (93-31)	Plateau age		Foster et al., 2001
Bitterroot Mylonite	Bitterroot	700		47.9	0.9							M3 metamorphism (exhumation)	House et al., 1997
Exhumation	Bitterroot	200		46.4	0.8	k-feldspar		40Ar/39Ar		rhyolitic dike, cross cuts mylonite, undeformed	southern Bitterroot mylonite	Intrusive age; minimum age of mylonitization	Hodges & Applegate, 1993
Exhumation	Bitterroot	200		45.4	0.2	k-feldspar		40Ar/39Ar		rhyolitic dike, cross cuts mylonite, undeformed (H&A,1993)	isochron age		Foster et al., 2001
Exhumation	Bitterroot	300		45	0.9	biotite		40Ar/39Ar		amhibolite pod (NB5-1); concordant but not mylonitic	isochron age	Rapid cooling	House & Hodges, 1994
Exhumation	Bitterroot	400		44.7	0.9	muscovite		40Ar/39Ar		protomylonitic schist (NB20-1)	isochron age	Rapid cooling	House & Hodges, 1994
Exhumation	Bitterroot	300		44.6	0.9	biotite		40Ar/39Ar		protomylonitic schist (NB20-1)	isochron age	Rapid cooling	House & Hodges, 1994
Exhumation	Bitterroot	300		44.3	0.9	biotite		40Ar/39Ar		amhibolite pod (NB17-1); concordant but not mylonitic	isochron age	Rapid cooling	House & Hodges, 1994
Exhumation	Bitterroot	300		44.1	0.9	biotite		40Ar/39Ar		mylonitic schist (NB16-4)	isochron age	Rapid cooling	House & Hodges, 1994
Exhumation	Bitterroot	400		44.0	0.2	muscovite		40Ar/39Ar		protomylonitic two-mica granodiorite, Lost Horse	Plateau age		Foster et al., 2001
Exhumation	Bitterroot	110		44	2	apatite		Fission track		Skookum Butte			Foster & Raza, 2002
Exhumation	Bitterroot	300		43.6	0.4	biotite		40Ar/39Ar		protomylonitic two-mica granodiorite, Lost Horse	Plateau age		Foster et al., 2001
Exhumation	Bitterroot	400		43.4	0.3	muscovite		40Ar/39Ar		protomylonitic two-mica granodiorite, Lost Horse	Plateau age		Foster et al., 2001
Exhumation	Bitterroot	300		43	0.2	biotite		40Ar/39Ar		protomylonitic two-mica granodiorite, Lost Horse	Plateau age		Foster et al., 2001
Exhumation	Bitterroot	300		42.9	0.8	biotite		40Ar/39Ar		unfoliated granitoid (NB4-1), structurally deepest	isochron age	Rapid cooling	House & Hodges, 1994
Exhumation	Bitterroot	400		42.6	0.8	muscovite		40Ar/39Ar		Sweathouse Canyon pegmatite	Plateau age		Foster et al., 2001
Exhumation	Bitterroot	400		42.4	0.8	muscovite		40Ar/39Ar		Sweathouse Canyon pegmatite	Plateau age		Foster et al., 2001
Exhumation	Bitterroot	400		42.2	0.8	muscovite		40Ar/39Ar		mylonitic schist (NB16-4)	isochron age	Rapid cooling	House & Hodges, 1994
Exhumation	Bitterroot	400		42.1	0.8	muscovite		40Ar/39Ar		mylonitic schist (NB16-1)	isochron age	Rapid cooling	House & Hodges, 1994
Exhumation	Bitterroot	300		42	0.3	biotite		40Ar/39Ar		biotite schist, Saint Mary's Peak	Plateau age		Foster et al., 2001
Exhumation	Bitterroot	200		42	4	zircon		Fission track		Boulder Creek			Foster & Raza, 2002
Exhumation	Bitterroot	110		41	2	apatite		Fission track		Skookum Butte			Foster & Raza, 2002
Exhumation	Bitterroot	110		41	1	apatite		Fission track		Skookum Butte			Foster & Raza, 2002
Exhumation	Bitterroot	200		40.3	0.8	k-feldspar		40Ar/39Ar		unfoliated granitoid (NB4-1), structurally deepest	isochron age	Rapid cooling	House & Hodges, 1994
Exhumation	Bitterroot	200		40	4	zircon		Fission track		Lost Horse Canyon			Foster & Raza, 2002
Exhumation	Bitterroot	200		39	0.7	k-feldspar		40Ar/39Ar		Sweathouse Canyon pegmatite	Plateau age, minimum		Foster et al., 2001
Exhumation	Bitterroot	110		39	3	apatite		Fission track		Lost Horse Canyon			Foster & Raza, 2002
Exhumation	Bitterroot	110		37	2	apatite		Fission track		Sapphire Mountains, hanging wall			Foster & Raza, 2002
Exhumation	Bitterroot	110		34	3	apatite		Fission track		Trapper Peak			Foster & Raza, 2002
Exhumation	Bitterroot	110		34	3	apatite		Fission track		Trapper Peak			Foster & Raza, 2002
Exhumation	Bitterroot	110		32	3	apatite		Fission track		Lost Horse Canyon			Foster & Raza, 2002
Exhumation	Bitterroot	110		31	2	apatite		Fission track		Lost Horse Canyon			Foster & Raza, 2002
Exhumation	Bitterroot	110		30	2	apatite		Fission track		Lost Horse Canyon			Foster & Raza, 2002
Exhumation	Bitterroot	110		30	3	apatite		Fission track		Lost Horse Canyon			Foster & Raza, 2002
Exhumation	Bitterroot	110		29	2	apatite		Fission track		Sweathouse Creek			Foster & Raza, 2002
Exhumation	Bitterroot	110		26	2	apatite		Fission track		Sweathouse Creek			Foster & Raza, 2002
Exhumation	Bitterroot	110		26	2	apatite		Fission track		Canyon Creek			Foster & Raza, 2002
Exhumation	Bitterroot	110		25	2	apatite		Fission track		Lost Horse Canyon			Foster & Raza, 2002
Exhumation	Bitterroot	110		25	2	apatite		Fission track		Sweathouse Creek			Foster & Raza, 2002
Exhumation	Bitterroot	110		24	2	apatite		Fission track		Sweathouse Creek			Foster & Raza, 2002
Exhumation	Bitterroot	110		24	2	apatite		Fission track		Canyon Creek			Foster & Raza, 2002
Exhumation	Bitterroot	110		24	3	apatite		Fission track		Bass Canyon			Foster & Raza, 2002
Exhumation	Bitterroot	110		23	3	apatite		Fission track		Lost Horse Canyon			Foster & Raza, 2002
Exhumation	Bitterroot	110		22	3	apatite		Fission track		Lost Horse Canyon			Foster & Raza, 2002
Exhumation	Bitterroot	110		19	2	apatite		Fission track		Blodget Canyon			Foster & Raza, 2002
M3	Clearwater	650		67		zircon		U-Pb		quartzite		Internal zone metamorphism - only one grain	Doughty et al., 2007
M3	Clearwater	650		64.2	2	zircon		U-Pb	SHRIMP	quartz-rich schists, internal zone, Jug Rock shear zone		first pulse of metamorphism (64)	Doughty et al., 2007
M3	Clearwater	650		64	1	zircon		U-Pb lower intercept	SHRIMP	garnet amphibolite, Moses Butte, internal zone		first pulse of metamorphism (64)	Doughty et al., 2007
M3	Clearwater	650		63.5	2.6	zircon		U-Pb	SHRIMP	quartz-rich schists, internal zone, Jug Rock shear zone		first pulse of metamorphism (64)	Doughty et al., 2007
M3	Clearwater	650		59	1.9	zircon		U-Pb lower intercept	SHRIMP	garnet amphibolite, Moses Butte, internal zone		second pulse of metamorphism (59-55), M3 - beginning of exhumation	Doughty et al., 2007
Cooling	Clearwater	400		57.8	3.2	muscovite		40Ar/39Ar		Schist of Monumental Buttes, external zone	Total fusion age		Doughty et al., 2007
Cooling	Clearwater	400		53.7	2.5	muscovite		40Ar/39Ar		Schist of Monumental Buttes, external zone	Inverse isochron		Doughty et al., 2007
Cooling	Clearwater	400		52.5	2.1	muscovite		40Ar/39Ar		Schist of Goat Mountain, internal zone	Plateau age		Doughty et al., 2007

Cooling	Clearwater	400		48	2.1	muscovite		40Ar/39Ar		Schist	total fusion age		Guevara, 2012
Cooling	Clearwater	300		47.2	0.8	biotite		40Ar/39Ar		Roundtop pluton, external zone	Plateau age		Doughty et al., 2007
Cooling	Clearwater	300		46.5	1	biotite		40Ar/39Ar		foliated granitoid, external zone	Plateau age		Doughty et al., 2007
Cooling	Clearwater	400		44.1	3.4	muscovite		40Ar/39Ar		quartzite	total fusion age		Guevara, 2012
Cooling	Clearwater	300		42.4	0.5	biotite		40Ar/39Ar		foliated granitoid, external zone	Plateau age		Doughty et al., 2007
Cooling	Clearwater	300		41.4	0.7	biotite		40Ar/39Ar		foliated granitoid, external zone	Plateau age		Doughty et al., 2007
Metamorphism	Priest River	785		64		monazite	spot	Th-Pb, REE	LASS	Hauser Lake Gneiss	HREE depleted porphyroblast inclusions	Peak metamorphism	Stevens et al., 2015
Metamorphism	Priest River	790		64		monazite	spot	Th-Pb, REE	LASS	Hauser Lake Gneiss	HREE depleted porphyroblast inclusions	Peak metamorphism	Stevens et al., 2015
Exhumation	Priest River	785		60		monazite	spot	Th-Pb, REE	LASS	Hauser Lake Gneiss	HREE enriched monazite analyses	Begin (early) garnet breakdown, decompression	Stevens et al., 2015
Exhumation	Priest River	785		57		monazite	spot	Th-Pb, REE	LASS	Hauser Lake Gneiss	HREE enriched monazite analyses	Begin (late) garnet breakdown, decompression	Stevens et al., 2015
Exhumation	Priest River	785		54								End isothermal decompression	Stevens et al., 2015
Exhumation	Priest River	540		51.59	2.01	hornblende		40Ar/39Ar		93-142 -- need 1995 dissertation	Plateau age		Doughty & Price, 1999
Exhumation	Priest River	400		50.13	0.3	muscovite		40Ar/39Ar		93-439 -- need 1995 dissertation	Plateau age		Doughty & Price, 1999
Exhumation	Priest River	300		49.86	0.33	biotite		40Ar/39Ar		93-26 -- need 1995 dissertation	Plateau age		Doughty & Price, 1999
Exhumation	Priest River	400		49.85	0.38	muscovite		40Ar/39Ar		93-26 -- need 1995 dissertation	Plateau age		Doughty & Price, 1999
Exhumation	Priest River	300		49.8	0.33	biotite		40Ar/39Ar		93-439 -- need 1995 dissertation	Plateau age		Doughty & Price, 1999
Exhumation	Priest River	300		48.69	0.73	biotite		40Ar/39Ar		Granite - southern footwall	Plateau age, reverse discordance		Doughty & Price, 2000
Exhumation	Priest River	540		48.09	3.28	hornblende		40Ar/39Ar		AFC2 -- need 1995 dissertation	Plateau age		Doughty & Price, 1999
Exhumation	Priest River	400		47.1	0.49	muscovite		40Ar/39Ar		92-260 -- need 1995 dissertation	Plateau age		Doughty & Price, 1999
Exhumation	Priest River	300		46.77	0.43	biotite		40Ar/39Ar		92-260 -- need 1995 dissertation	Plateau age		Doughty & Price, 1999
Exhumation	Priest River	200		46.06	1.05	k-feldspar		40Ar/39Ar		PRAG -- need 1995 dissertation	Plateau age		Doughty & Price, 1999
Exhumation	Priest River	400		45.37	1.17	muscovite		40Ar/39Ar		Granite - southern footwall	Plateau age, reverse discordance		Doughty & Price, 2000
Prograde	Valhalla	820		80		monazite		U-Pb	ID-TIMS	paragneiss, Gwillim Creek		Beginning of high-grade metamorphism	Spear & Parrish, 1996
Prograde	Valhalla	820	30	75					geothermobarometry	Ladybird granite and paragneiss	5-20% melt; Prograde muscovite dehydration melting		Spear & Parrish, 1996
Prograde	Valhalla	650	26	74		allanite		U-Pb	ID-TIMS		closure temperature		Spear & Parrish, 1996
Peak	Valhalla	600	25	61		titanite		U-Pb	ID-TIMS	Mulvey gneiss	closure temperature		Spear & Parrish, 1996
Peak	Valhalla	540		60.3	0.5	hornblende		40Ar/39Ar		amphibolite	preferred age		Gordon et al., 2008
Peak	Valhalla	825		60					geothermobarometry	Metapelite, Domain I		Near-thermal peak	Schaubs et al., 2002
Peak	Valhalla	815		60					geothermobarometry	Amphibolite, Domain I		Near-thermal peak	Schaubs et al., 2002
Peak	Valhalla	850		60					geothermobarometry	Domain V-II		Near-thermal peak	Schaubs et al., 2002
Peak	Valhalla	725		60					geothermobarometry	Amphibolite gneisses, Domains V-I, P-I	average results	Near-thermal peak	Schaubs et al., 2002
Exhumation	Valhalla	300		57.7	0.7	biotite		40Ar/39Ar		leucogranite	preferred age		Gordon et al., 2008
Exhumation	Valhalla	400		55	1	muscovite		Rb-Sr			closure temperature		Spear & Parrish, 1996
Exhumation	Valhalla	400		54.7	1.1	muscovite		40Ar/39Ar		grt-bearing paragneiss	preferred age		Gordon et al., 2008
Exhumation	Valhalla	500		54.5	1	muscovite		Rb-Sr		Ladybird granite, mylonitized		age of late greenschist mylonitization	Parrish et al., 1988
Exhumation	Valhalla	540		54.3	0.4	hornblende		40Ar/39Ar		amphibolite	preferred age		Gordon et al., 2008
Exhumation	Valhalla	400		53.1	0.3	biotite		40Ar/39Ar		leucogranite	preferred age		Gordon et al., 2008
Exhumation	Valhalla	400		51.4	0.4	biotite		40Ar/39Ar		leucosome, boudin neck	preferred age		Gordon et al., 2008
Exhumation	Valhalla	650		51	2	zircon	depth	U-Pb	ion microprobe			beginning of exhumation	Gordon et al., 2008
Exhumation	Valhalla	400		50.6	0.2	biotite		40Ar/39Ar		quartzofeldspathic gneiss, migmatitic	preferred age		Gordon et al., 2008
Exhumation	Valhalla	400		48.8	0.4	biotite		40Ar/39Ar		grt-bearing migmatitic paragneiss	preferred age		Gordon et al., 2008
Exhumation	Valhalla	400		48.6	0.5	biotite		40Ar/39Ar		grt-bearing paragneiss	preferred age		Gordon et al., 2008
Exhumation	Valhalla	400		48.1	0.5	biotite		40Ar/39Ar		leucosome, boudin neck	preferred age		Gordon et al., 2008
Exhumation	Valhalla	110	10	44		apatite		fission track			closure temperature		Spear & Parrish, 1996
Metamorphism	Thor-Odin	750		56						Gedrite-cordierite rock			Norlander et al., 2002
Metamorphism	Thor-Odin	800		56						Metapelitic gneiss			Norlander et al., 2002
Metamorphism	Thor-Odin	750		56						garnet-hornblende amphibolite			Norlander et al., 2002
Metamorphism	Thor Odin	750		56					pseudosection				Goergen and Whitney, 2012
Metamorphism	Thor-Odin	750		50								Isothermal decompression to this level (10 to 4-5 kbar at 700-800C)	Norlander et al., 2002
Cooling	Thor-Odin	540		59		hornblende		40Ar/39Ar			max in range		Vanderhaeghe et al., 1999
Cooling	Thor-Odin	540		53.7		hornblende		40Ar/39Ar			min in range		Vanderhaeghe et al., 1999
Cooling	Thor-Odin	350		49.5		mica		40Ar/39Ar			max in range	End of rapid cooling event following rapid exhumation	Vanderhaeghe et al., 1999
Cooling	Thor-Odin	220	50	49.2	4	zircon	multi	fission track					Lorencak et al., 2001
Cooling	Thor-Odin	110	10	48.5	3.2	apatite	multi	fission track					Lorencak et al., 2001
Cooling	Thor-Odin	220	50	48.2	3.4	zircon	multi	fission track					Lorencak et al., 2001
Cooling	Thor-Odin	350		47.7		mica		40Ar/39Ar			min in range		Vanderhaeghe et al., 1999
Cooling	Thor-Odin	110	10	46.1	3.8	apatite	multi	fission track					Lorencak et al., 2001
Cooling	Thor-Odin	220	50	44.3	4	zircon	multi	fission track					Lorencak et al., 2001
Cooling	Thor-Odin	110	10	43.7	4	apatite	multi	fission track					Lorencak et al., 2001
Cooling	Thor-Odin	200		43		K-feldspar		40Ar/39Ar			min in range		Vanderhaeghe et al., 1999
Cooling	Thor-Odin	110	10	39.5	3.2	apatite	multi	fission track					Lorencak et al., 2001
Cooling	Thor-Odin	200		33		K-feldspar		40Ar/39Ar				End of rapid cooling following high angle normal faulting	Vanderhaeghe et al., 1999
Cooling	Thor-Odin	110	10	30.2	2.8	apatite	multi	fission track					Lorencak et al., 2001
Cooling	Thor-Odin	110	10	27.7	3.4	apatite	multi	fission track					Lorencak et al., 2001

Does not include K-Ar data.
Data with larger errors not included.

Reference List

Doughty, P. T. and Price, R. A., 1999, Tectonic evolution of the Priest River complex, northern Idaho and Washington: A reappraisal of the Newport fault with new insights on metamorphic core complex formation: Tectonics, v. 18, no. 3, p. 375-393.

Doughty, P. T. and Price, R. A., 2000, Geology of the Purcell Trench rift valley and Sandpoint Conglomerate: Eocene en echelon normal faulting and synrift sedimentation along the eastern flank of the Priest River metamorphic complex, northern Idaho: Geological Society of America Bulletin, v. 112, no. 9, p. 1356-1374.

Doughty, P. T., Chamberlain, K. R., Foster, D. A., and Sha, G. S., 2007, Structural, metamorphic, and geochonologic constraints on the origin of the Clearwater core complex, northern Idaho. In: Whence the Mountains? Inquiries into the Evolution of Orogenic Systems: A Volume in Honor of Raymond A. Price (eds Sears, J. W., Harms, T. A. & Evenchick, C. A.) Geological Society of America Special Paper, pp. 211-241, Geological Society of America, Boulder, Colorado.

Foster, D. A. & Raza, A., 2002. Low-temperature thermochronological record of exhumation of the Bitterroot metamorphic core complex, northern Cordilleran Orogen, pp. 23-36.

Foster, D. A., Schafer, C., Fanning, C. M. & Hyndman, D. W., 2001. Relationships between crustal partial melting, plutonism, orogeny, and exhumation: Idaho-Bitterroot batholith. Tectonophysics, 342, 313-350.

Goergen, E. T. & Whitney, D. L., 2011. Long length scales of element transport during reaction texture development in orthoamphibole-cordierite gneiss: Thor-Odin dome, British Columbia, Canada. Contributions to Mineralogy and Petrology, 163(2), 337-352.

Gordon, S. M., Whitney, D. L., Teyssier, C., Grove, M. & Dunlap, W. J., 2008. Timescales of migmatization, melt crystallization, and cooling in a Cordilleran gneiss dome: Valhalla complex, southeastern British Columbia. Tectonics, 27(4), TC4010.

Guevara, V. E., 2012. Structural, Thermochronological, and Stratigraphic Constraints on the Evolution of the Clearwater Metamorphic Core Complex, Idaho, University of Montana, Missoula, Montana.

Hodges, K. V. & Applegate, J. D., 1993. Age of Tertiary extension in the Bitterroot metamorphic core complex, Montana and Idaho. Geology, 21(2), 161-164.

House, M. A. & Hodges, K. V., 1994. Limits on the tectonic significance of rapid cooling events in extensional settings - insights from the Bitterroot metamorphic core complex, Idaho-Montana. Geology, 22(11), 1007-1010.

House, M. A., Hodges, K. V. & Bowring, S. A., 1997. Petrological and geochronological constraints on regional metamorphism along the northern border of the Bitterroot batholith. Journal of Metamorphic Geology, 15(6), 753-764.

House, M. A., Bowring, S. A. & Hodges, K. V., 2002. Implications of middle Eocene epizonal plutonism for the unroofing history of the Bitterroot metamorphic core complex, Idaho-Montana. Geological Society of America Bulletin, 114(4), 448-461.

Lorencak, M., Seward, D., Vanderhaeghe, O., Teyssier, C. & Burg, J. P., 2001. Low-temperature cooling history of the Shuswap metamorphic core complex, British Columbia: constraints from apatite and zircon fission-track ages. Canadian Journal of Earth Sciences, 38(11), 1615-1625.

Norlander, B. H., Whitney, D. L., Teyssier, C. & Vanderhaeghe, O., 2002. Partial melting and decompression of the Thor-Odin dome, Shuswap metamorphic core complex, Canadian Cordillera. Lithos, 61, 103-125.

Parrish, R. R., Carr, S. D. & Parkinson, D. L., 1988. Eocene extensional tectonics and geochronology of the southern Omineca Belt, British Columbia and Washington. Tectonics, 7(2), 181-212.

Schaubs, P. M., Carr, S. D. & Berman, R. G., 2002. Structural and metamorphic constraints on ca. 70 Ma deformation of the northern Valhalla complex, British Columbia: implications for the tectonic evolution of the southern Omineca belt. Journal of Structural Geology, 24, 1195-1214.

Spear, F. S. & Parrish, R. R., 1996. Petrology and cooling rates of the Valhalla complex, British Columbia, Canada. Journal of Petrology, 37(4), 733-765.

Stevens, L. M., Baldwin, J. A., Cottle, J. M. & Kylander-Clark, A. R. C., 2015. Phase equilibria modelling and LASS monazite petrochronology:P-T-tconstraints on the evolution of the Priest River core complex, northern Idaho. Journal of Metamorphic Geology, 33(4), 385-411.

Vanderhaeghe, O., Teyssier, C. & Wysoczanski, R., 1999. Structural and geochronological constraints on the role of partial melting during the formation of the Shuswap metamorphic core complex at the latitude of the Thor-Odin dome, British Columbia. Canadian Journal of Earth Sciences, 36, 917-943.